



This is a repository copy of *Predictive control design on an embedded robust output-feedback compensator for wind turbine blade-pitch preview control*.

White Rose Research Online URL for this paper:
<http://eprints.whiterose.ac.uk/101834/>

Version: Accepted Version

Proceedings Paper:

Lio, W.H. orcid.org/0000-0002-3946-8431, Rossiter, J.A. and Jones, B.L. (2016) Predictive control design on an embedded robust output-feedback compensator for wind turbine blade-pitch preview control. In: European Control Conference 2016. European Control Conference 2016, 29 Jun - 01 Jul 2016 . ISBN 978-1-5090-2590-9

Reuse

Unless indicated otherwise, fulltext items are protected by copyright with all rights reserved. The copyright exception in section 29 of the Copyright, Designs and Patents Act 1988 allows the making of a single copy solely for the purpose of non-commercial research or private study within the limits of fair dealing. The publisher or other rights-holder may allow further reproduction and re-use of this version - refer to the White Rose Research Online record for this item. Where records identify the publisher as the copyright holder, users can verify any specific terms of use on the publisher's website.

Takedown

If you consider content in White Rose Research Online to be in breach of UK law, please notify us by emailing eprints@whiterose.ac.uk including the URL of the record and the reason for the withdrawal request.



eprints@whiterose.ac.uk
<https://eprints.whiterose.ac.uk/>

Predictive control design on an embedded robust output-feedback compensator for wind turbine blade-pitch preview control

Wai Hou Lio, J.A. Rossiter and Bryn Ll. Jones

Abstract—The use of upstream wind measurements has motivated the development of blade-pitch preview controllers to improve rotor speed tracking and structural load reduction beyond that achievable via conventional feedback design. Such preview controllers, typically based upon model predictive control (MPC) for its constraint handling properties, alter the closed-loop dynamics of the existing blade-pitch feedback control system. This can result in the robustness properties of the original closed-loop system being no longer preserved. As a consequence, the aim of this work is to formulate a MPC layer on top of a given output-feedback controller, with a view to retaining the closed-loop robustness and frequency-domain performance of the latter. The separate nature of the proposed controller structure enables clear and transparent qualifications of the benefits gained by using preview and predictive control. This is illustrated by results obtained from closed-loop simulations upon a high-fidelity turbine, showing the performance comparison between a nominal feedback compensator and the proposed MPC-based preview controller.

I. INTRODUCTION

The rotor and structural components of large wind turbines are subjected to unsteady and intermittent aerodynamic loads from the wind. Such unsteady loads cause the rotor speed and power generation to exceed the design specification and also lead to fatigue damage to key turbine structural components, resulting in a reduction of the operational lifetime. Most wind turbines are equipped with blade-pitch controllers for achieving turbine speed regulation in above-rated wind conditions. An increasing number of large wind turbines are beginning to exploit the adjustment of blade pitch angle to attenuate unbalanced loads on the rotor. These two strategies are commonly known as: (i) collective pitch control (CPC), whose role is to regulate rotor speed by adjusting the pitch angle of each blade by the same amount, and (ii) individual pitch control (IPC), which provides an additional pitch angle demand signal, typically in response to measurement of flap-wise blade bending moments, to attenuate the effect of unsteady loads on the rotor (e.g. [1], [2]).

In recent years, a growing body of research has emerged, seeking to utilise real-time measurement of wind conditions from remote sensing devices for feed-forward control design. Some earlier results studied the use of preview control design for CPC (e.g. [3]) and suggested significant performance improvement over feedback-only designs; the first field test on feed-forward CPC design was reported by [4]. Lately, [5] investigated IPC design with advance wind knowledge and

concluded that the feed-forward IPC design should include a careful consideration of the pitch actuator activity. As a consequence, several authors (e.g. [6]–[8]), employed model predictive control (MPC) in a preview IPC design owing to its ability to handle constraints and feed-forward information, and their results demonstrated the efficacy of a preview MPC design in the flap-wise blade load reduction.

The majority of wind turbine preview MPC studies can be divided into two categories. The first branch is to formulate the blade-pitch control problem as one single MPC formulation where the resultant controller handles both feedback and feed-forward measurements (e.g. [7]), whilst the second branch is to construct the MPC layer based on a known state-feedback controller (e.g. [6]). The shortcomings of both methods are that the robustness and closed-loop frequency-domain properties are usually not well considered in a standard MPC design. The loads on turbine blades predominately exist at the harmonics of the blade rotational frequency, thus, it is not straightforward to design robust closed-loop feedback controllers in the time-domain. Furthermore, it is often assumed that the existing controllers use full state-feedback, despite the fact that output-feedback controllers are prevalent in industry.

This work therefore aims to bridge this gap by formulating a MPC layer based on a known robust output-feedback controller, where the MPC layer handles constraints and upcoming wind measurements. A further key focus of this paper stems from existing research often overlooking the conditions that separate the original closed-loop dynamics from the additional control layer design. If the given closed-loop dynamics are changed by the extra layer design, as a consequence, the benefits of utilising real-time measurement of the upstream wind become less transparent. The separate nature of the MPC layer is important from an industry perspective, since it can be implemented without replacing the existing feedback controller. Also, it provides a clear framework to quantify the benefits of feed-forward and predictive control over a baseline feedback strategy.

The remainder of this paper is structured as follows. In Section II, the modelling aspect of the blade pitch control problem, including disturbance modelling, is presented and the detail of the nominal embedded feedback controller is discussed. This is followed in Section III by a formulation of a predictive control layer and the conditions that ensure the original closed-loop dynamics are retained which is the main result of this paper. In Section IV, simulation results on a high-fidelity wind turbine demonstrate the benefits of having the proposed MPC layer on top of the closed-loop

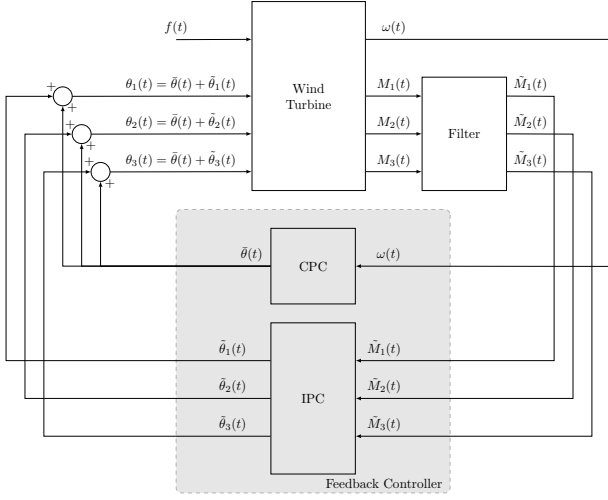


Fig. 1. System architecture of a wind turbine blade-pitch control system, combining of collective pitch control (CPC) and individual pitch control (IPC). The CPC regulates rotor speed while the IPC attenuates perturbations in the flap-wise root bending moments on each blade. Additional inputs to the turbine, such as wind loading and generator torque, are accounted for in the term $f(t)$

feedback controller. Conclusions are in Section V.

II. WIND TURBINE MODELLING AND NOMINAL ROBUST FEEDBACK COMPENSATOR

This section presents background on the wind turbine model and disturbances. In addition, the details of the embedded nominal robust feedback controller are discussed.

A. Wind turbine modelling

A typical wind turbine blade pitch control system architecture for above-rated conditions is depicted in Figure 1. The CPC regulates the rotor speed $\omega(t)$ by adjusting the collective pitch angle signal whilst the IPC attenuates loads by providing additional pitch signals on top of the collective pitch angle in response to flap-wise blade root bending moment signals. To isolate the action of the IPC from the CPC (e.g. [1], [9]–[11]), it is convenient to define the pitch angles and blade moments as follows:

$$\begin{bmatrix} \theta_1(t) \\ \theta_2(t) \\ \theta_3(t) \end{bmatrix} := \begin{bmatrix} \bar{\theta}(t) + \tilde{\theta}_1(t) \\ \bar{\theta}(t) + \tilde{\theta}_2(t) \\ \bar{\theta}(t) + \tilde{\theta}_3(t) \end{bmatrix}, \quad \begin{bmatrix} M_1(t) \\ M_2(t) \\ M_3(t) \end{bmatrix} := \begin{bmatrix} \bar{M}(t) + \tilde{M}_1(t) \\ \bar{M}(t) + \tilde{M}_2(t) \\ \bar{M}(t) + \tilde{M}_3(t) \end{bmatrix} \quad (1)$$

For simplicity, it is assumed that there is no coupling between the CPC and IPC loops from the tower dynamics. The relationship between collective pitch input $\bar{\theta}(t)$ and rotor speed output $\omega(t)$ can be modelled by a transfer function $G_{\omega\theta}(s)$ obtained by linearising the turbine dynamics around the operating wind condition of 18 ms^{-1} , chosen because this value is close to the centre of the range of wind speeds covering the above-rated wind condition. Similarly, the relationship mapping the perturbations in flap-wise blade root bending moment $\tilde{M}_{1,2,3}$ to additional pitch angle $\tilde{\theta}_{1,2,3}$ of

each blade can be modelled by a transfer function $G_{M\theta}(s)$. These transfer functions are as follows:

$$G_{\omega\theta}(s) := G_a(s)G_r(s), \quad (2a)$$

$$G_{M\theta}(s) := G_a(s)G_b(s)G_{bp}(s), \quad (2b)$$

where $G_r(s)$, $G_b(s)$ and $G_a(s)$ describe the dynamics of rotor, blade and actuator, respectively, whilst $G_{bp}(s)$ is a band-pass filter that is included in order to remove the low and high frequency contents of the blade root bending measurement signals, obtained from strain-gauge sensors. These transfer functions are defined as follows:

$$G_r(s) := \frac{\partial\omega}{\partial\theta} \frac{1}{\tau_r s + 1}, \quad (3a)$$

$$G_b(s) := \frac{\partial M_{\text{flap}}}{\partial\theta} \frac{(2\pi f_b)^2}{s^2 + 4\pi f_b D_b s + (2\pi f_b)^2}, \quad (3b)$$

$$G_a(s) := \frac{1}{\tau_s + 1}, \quad (3c)$$

$$G_{bp}(s) := \frac{2\pi f_h}{s^2 + 2\pi(f_h + f_l)s + 4\pi^2 f_h f_l}, \quad (3d)$$

where $\frac{\partial\omega}{\partial\theta}$ and τ_r denote the the variation in rotor speed to pitch angle and time constant of the rotor dynamics, whilst $\frac{\partial M_{\text{flap}}}{\partial\theta}$, D_b and f_b represent change in blade bending moment to pitch angle, blade damping ratio and natural frequency of first blade mode, respectively. The time constant of the pitch actuator is τ whilst f_h and f_l denote the upper and lower cut-off frequencies of the band-pass filter, respectively. Values are listed in Table II.

B. Disturbance modelling

The rotor and blade are subjected to a temporally varying and spatially distributed wind field. Given the feasibility of estimating the wind-field from a few point measurements taken upstream of the turbine (e.g. [12]), this work assumes the full approaching wind field is known a priori. The disturbance trajectories of rotor speed ω_d and flap-wise blade bending moment \tilde{M}_{d_i} , for $i \in \{1, 2, 3\}$, caused by the approaching wind, are defined as follows:

$$\omega_d(k) := \sum_{l,\phi} \frac{\partial\omega}{\partial v}(\bar{v}, l)v(l, \phi) \quad (4)$$

$$\tilde{M}_{d_i}(k) := \sum_{l,\phi} \frac{\partial M_{\text{flap}}}{\partial v}(\bar{v}, l)v(l, \phi), \quad i = 1, 2, 3 \quad (5)$$

where $v(l, \phi)$ denote the stream-wise wind speed measurements where l and ϕ represent the radial and angular coordinates across the rotor disk whilst \bar{v} denote the averaged wind speed of the measurements. Noted that span-wise and vertical wind speed is assumed negligible because the turbine blades spin fast in span-wise and vertical directions. The variations in rotor speed and blade bending moment with respect to the wind are denoted as $\frac{\partial\omega_d}{\partial v}$ and $\frac{\partial M_{d_i}}{\partial v}$. The rotor speed response ω to wind-induced disturbance ω_d is modelled as a first-order transfer function $G_{\omega\omega_d}(s)$, whilst the response of flap-wise blade root bending moment \tilde{M}_i to wind-induced disturbance \tilde{M}_{d_i} , for $i \in \{1, 2, 3\}$, is modelled as $G_{MM_d}(s)$:

$$G_{\omega\omega_d}(s) := \frac{1}{\tau_r s + 1}, \quad (6a)$$

$$G_{MM_d}(s) := \frac{(2\pi f_b)^2}{s^2 + 4\pi f_b D_b s + (2\pi f_b)^2} G_{bp}(s), \quad (6b)$$

Combining (2) and (6), the overall transfer function models $G(s)$ and $G_d(s)$ can be represented as follows:

$$\begin{aligned} \begin{bmatrix} \omega(s) \\ \tilde{M}_1(s) \\ \tilde{M}_2(s) \\ \tilde{M}_3(s) \end{bmatrix} &= \underbrace{\begin{bmatrix} G_{\omega\theta}(s) & 0 & 0 & 0 \\ 0 & G_{M\theta}(s) & 0 & 0 \\ 0 & 0 & G_{M\theta}(s) & 0 \\ 0 & 0 & 0 & G_{M\theta}(s) \end{bmatrix}}_{G(s)} \begin{bmatrix} \bar{\theta}(s) \\ \tilde{\theta}_1(s) \\ \tilde{\theta}_2(s) \\ \tilde{\theta}_3(s) \end{bmatrix} \\ + \underbrace{\begin{bmatrix} G_{\omega\omega_d}(s) & 0 & 0 & 0 \\ 0 & G_{MM_d}(s) & 0 & 0 \\ 0 & 0 & G_{MM_d}(s) & 0 \\ 0 & 0 & 0 & G_{MM_d}(s) \end{bmatrix}}_{G_d(s)} &\begin{bmatrix} \omega_d(s) \\ \tilde{M}_{d1}(s) \\ \tilde{M}_{d2}(s) \\ \tilde{M}_{d3}(s) \end{bmatrix} \end{aligned} \quad (7)$$

Equivalently, a discrete-time state-space model representation can be constructed as follows:

$$x_{k+1}^p = A^p x_k^p + B^p u_k + B_d^p d_k, \quad (8a)$$

$$y_k = C^p x_k^p, \quad (8b)$$

$$u_k = [\bar{\theta}_k, \tilde{\theta}_{1k}, \tilde{\theta}_{2k}, \tilde{\theta}_{3k}]^T, \quad (8c)$$

$$y_k = [\omega_k, \tilde{M}_{1k}, \tilde{M}_{2k}, \tilde{M}_{3k}]^T, \quad (8d)$$

$$d_k = [\omega_{dk}, \tilde{M}_{d1k}, \tilde{M}_{d2k}, \tilde{M}_{d3k}]^T, \quad (8e)$$

where superscript p denotes plant.

C. Nominal embedded robust feedback controller

The chosen robust feedback controller $K(s)$, consisting of the CPC $K_{\theta\omega}(s)$ and the IPC $K_{\theta M}(s)$, employed in this work is defined as follows:

$$\begin{bmatrix} \bar{\theta}(s) \\ \tilde{\theta}_1(s) \\ \tilde{\theta}_2(s) \\ \tilde{\theta}_3(s) \end{bmatrix} = \underbrace{\begin{bmatrix} K_{\theta\omega}(s) & 0 & 0 & 0 \\ 0 & K_{\theta M}(s) & 0 & 0 \\ 0 & 0 & K_{\theta M}(s) & 0 \\ 0 & 0 & 0 & K_{\theta M}(s) \end{bmatrix}}_{K(s)} \begin{bmatrix} \omega(s) \\ \tilde{M}_1(s) \\ \tilde{M}_2(s) \\ \tilde{M}_3(s) \end{bmatrix} \quad (9)$$

where $K_{\theta\omega}(s)$ and $K_{\theta M}(s)$ obtained from [11], are presented in Appendix I. It is assumed no dynamic coupling exists between the fixed and rotating turbine structures. The simulation results in [11] showed that a controller of the form (9) could be designed to be insensitive to such coupling by shaping the open-loop frequency response to have low gain at the tower frequency. Similar to the plant model, the nominal feedback controller (9) in a discrete time state-space realisation is:

$$x_{k+1}^\kappa = A^\kappa x_k^\kappa - B^\kappa y_k, \quad (10a)$$

$$u_k = C^\kappa x_k^\kappa - D^\kappa y_k, \quad (10b)$$

where the vector x^κ represents the state of the controller and the superscript κ denotes controller.

III. FORMULATION OF THE MPC LAYER

The architecture combining the proposed MPC layer and the nominal feedback controller is shown in Figure 2, where the shaded area depicts the existing closed-loop system. The closed-loop system dynamics in a state-augmented form can

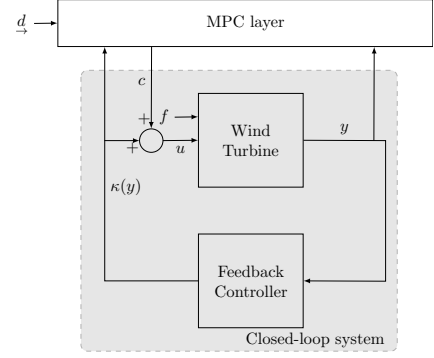


Fig. 2. Concept of model predictive control layer on top of a known feedback controller.

be derived from the discrete-time state-space wind turbine model (8) and the feedback controller (10):

$$\begin{bmatrix} x_{k+1}^p \\ x_{k+1}^\kappa \\ u_k \end{bmatrix} = \underbrace{\begin{bmatrix} A^p & 0 & B^p \\ -B^\kappa C^p & A^\kappa & 0 \\ 0 & 0 & I \end{bmatrix}}_A \underbrace{\begin{bmatrix} x_k^p \\ x_k^\kappa \\ u_{k-1} \end{bmatrix}}_{x_k} + \underbrace{\begin{bmatrix} B^p \\ 0 \\ I \end{bmatrix}}_B \Delta u_k + \underbrace{\begin{bmatrix} B_d^p \\ 0 \\ 0 \end{bmatrix}}_{B_d} d_k \quad (11a)$$

$$\Delta u_k = K x_k = \begin{bmatrix} -D^\kappa C^p & C^\kappa & -I \end{bmatrix} x_k \quad (11b)$$

$$y_k = C x_k = \begin{bmatrix} C^p & 0 & 0 \end{bmatrix} x_k \quad (11c)$$

Note that an incremental input Δu_k is employed in the state-augmented closed-loop system model (11a) as the input variable because of the simplicity of formulation of blade pitch rate and angle constraints.

A. Augmentation of input perturbations into the underlying feedback control law

The MPC formulation in this work adopts a closed-loop paradigm [13] where the degrees-of-freedom (d.o.f) c_k can be set up around the stabilising feedback control law (11b) $\Delta u_k = K x_k$ such that the input can be parametrised as $\Delta u_k = K x_k + c_k$ with the premise that the perturbation $c_k \neq 0$ if and only if constraints are active or feed-forward knowledge is available. Such a feature is particularly useful in formulating a MPC layer on top of an embedded closed-loop controller. The closed-loop paradigm employed in this work uses a dual-mode approach and these two modes of predictions are the transient mode and the terminal mode. In transient mode, a sequence of input d.o.f.s, denoted as $\vec{c}_k = [c_{0|k}, c_{1|k}, \dots, c_{n_c-1|k}]^T$, is optimised over the control horizon n_c in respect to handling of constraints and feed-forward information, whilst in the terminal mode, the closed-loop dynamics are governed by the pre-determined control law, which is the embedded robust feedback pitch controller in this case. Considering (11a), the predictions of input and state at sample time k can be described as follows:

$$\Delta u_{i|k} = \begin{cases} K x_{i|k} + c_{i|k}, & \forall i < n_c, \\ K x_{i|k}, & \forall i \geq n_c, \end{cases} \quad (12a)$$

$$x_{i+1|k} = \begin{cases} \Phi x_{i|k} + B c_{i|k} + B_d d_{i|k}, & \forall i < n_c, \\ \Phi x_{i|k} + B_d d_{i|k}, & \forall i \geq n_c, \end{cases} \quad (12b)$$

where $\Phi = A + BK$. Noted that $x_{0|k} = x_k$. The predictions of disturbance measurement $\underline{d}_{\rightarrow k} = [d_{0|k}, d_{1|k}, \dots, d_{n_a-1|k}]^T$ is defined as follows:

$$d_{i|k} = \begin{cases} d_{k+i}, & \forall i < n_a \\ 0, & \forall i \geq n_a. \end{cases} \quad (12c)$$

It is assumed that beyond the preview horizon n_a , the upcoming disturbance measurement becomes zero. Subsequently, it is more convenient to represent the dual-mode predictions in one autonomous model such that the model consists of state predictions (12b), input prediction sequence (12a) and advance disturbance measurement (12c). The autonomous model with the augmented state $z_{i|k}$ is defined as follows:

$$z_{i+1|k} = \Psi z_{i|k} \quad (13a)$$

where the initial augmented state $z_{0|k} = [x_{0|k}^T, \underline{c}_{\rightarrow k}^T, \underline{d}_{\rightarrow k}^T]^T$ and Ψ is defined as:

$$\Psi = \begin{bmatrix} \Phi & BE & B_d E \\ 0 & M_c & 0 \\ 0 & 0 & M_d \end{bmatrix}, \quad (13b)$$

$$E \underline{c}_{\rightarrow k} = c_{0|k}, E \underline{d}_{\rightarrow k} = d_{0|k}, \quad (13c)$$

$$M_c \underline{c}_{\rightarrow k} = [c_{1|k}^T, \dots, c_{n_c-1|k}^T, 0]^T, \quad (13d)$$

$$M_d \underline{d}_{\rightarrow k} = [d_{1|k}^T, \dots, d_{n_a-1|k}^T, 0]^T. \quad (13e)$$

Consequently, the prediction of state and input (employed in the cost function) can be expressed in terms of the autonomous model (13a) as follows:

$$x_{i|k} = \underbrace{[I \ 0 \ 0]}_{\Gamma_x} z_{i|k}, \quad \forall i \geq 0, \quad (14a)$$

$$\Delta u_{i|k} = \underbrace{[K \ E \ 0]}_{\Gamma_u} z_{i|k}, \quad \forall i \geq 0. \quad (14b)$$

B. Formulation of the cost function

The input perturbation sequence $\underline{c}_{\rightarrow k}$ is computed by solving a constrained minimisation of the predicted cost where the predicted cost function quantifying the balance between performance and input effort is defined as follows:

$$J := \sum_{i=0}^{\infty} \left[x_{i|k}^T Q x_{i|k} + \Delta u_{i|k}^T R \Delta u_{i|k} + 2x_{i|k}^T N \Delta u_{i|k} \right] \quad (15)$$

where Q , R and N denote the weighting matrices that specify the penalties on state and input in the cost. For practical reasons, the infinite-horizon cost function (15) needs to be expressed in a finite-horizon form such that it can be solved on-line rapidly by quadratic programming. By expressing the prediction of the deviation variables of state (14a) and input (14b) in terms of the autonomous model, the cost function (15) can be simplified as follows:

$$J := z_{0|k}^T \underbrace{\sum_{i=0}^{\infty} \Psi^i \Gamma_x^T Q \Gamma_x + \Gamma_u^T R \Gamma_u + 2\Gamma_x^T N \Gamma_u}_{\substack{W \\ S}} \Psi^i z_{0|k} \quad (16)$$

Consequently, the cost function (16) can be further simplified, using the Lyapunov equation $\Psi^T S \Psi = S - W$, as:

$$J := \begin{bmatrix} x_{0|k} \\ \underline{c}_{\rightarrow k} \\ \underline{d}_{\rightarrow k} \end{bmatrix}^T \underbrace{\begin{bmatrix} S_x & S_{xc} & S_{xd} \\ S_{xc}^T & S_c & S_{cd} \\ S_{xd}^T & S_{cd}^T & S_d \end{bmatrix}}_S \underbrace{\begin{bmatrix} x_{0|k} \\ \underline{c}_{\rightarrow k} \\ \underline{d}_{\rightarrow k} \end{bmatrix}}_{z_{0|k}} \quad (17)$$

C. Constraint formation in terms of input perturbations

The physical limits on pitch actuator rate and angle are considered as hard constraints in this work. The limits on pitch rate are ± 8 degrees per second, whilst the pitch angle is bounded between 0 degree and 90 degrees:

$$\Delta \underline{u} \leq \Delta u_{i|k} \leq \Delta \bar{u}, \quad \forall i \geq 0, \quad (18a)$$

$$\underline{u} \leq u_{i|k} \leq \bar{u}, \quad \forall i \geq 0. \quad (18b)$$

These inequalities can be written in terms of the autonomous model (13a), with $z_{i|k} = \Psi^i z_{0|k}$, as follows:

$$H \Psi^i z_{0|k} \leq f, \quad \forall i \geq 0. \quad (18c)$$

where $H z_{i|k} = [u_{i|k}, -u_{i|k}, \Delta u_{i|k}, -\Delta u_{i|k}]^T$ and $f = [\bar{u}, \underline{u}, \Delta \bar{u}, \Delta \underline{u}]^T$. It is noted that to ensure no constraint violations, possible violations must be checked over an infinite prediction horizon. Nevertheless, there exists a sufficiently large horizon where any additional linear equalities become redundant [14]. Consequently, for a practical approach, this study formulates the inequalities by checking the constraints over twice the control horizon and the inequalities can be described by a set of suitable matrices (\mathcal{M} , \mathcal{N} , \mathcal{V} and b) as follows:

$$\mathcal{M} x_k + \mathcal{N} \underline{c}_{\rightarrow k} + \mathcal{V} \underline{d}_{\rightarrow k} \leq b. \quad (19)$$

To sum up the discussion so far, the optimal input perturbation sequence $\underline{c}_{\rightarrow k}$ from the MPC layer can be computed by solving a minimisation of the predicted cost function (17) subject to constraints (19). This is summarised in Algorithm 1:

Algorithm 1: At each sampling instant perform the optimisation below. The first block element of the perturbation $\underline{c}_{\rightarrow k}$ is applied within the embedded control law (12a):

$$\min_{\underline{c}_{\rightarrow k}} \underline{c}_{\rightarrow k}^T S_c \underline{c}_{\rightarrow k} + 2 \underline{c}_{\rightarrow k}^T S_{xc}^T x_{0|k} + 2 \underline{c}_{\rightarrow k}^T S_{cd} \underline{d}_{\rightarrow k} \quad (20a)$$

$$\text{s.t. } \mathcal{M} x_k + \mathcal{N} \underline{c}_{\rightarrow k} + \mathcal{V} \underline{d}_{\rightarrow k} \leq b \quad (20b)$$

D. Key result - Conditions for separating the original closed-loop dynamics from the additional layer design

The unconstrained optimal input sequence can be obtained by solving the minimisation of the cost (17) as follows:

$$\underline{c}_{\rightarrow k} = -S_c^{-1} S_{xc}^T x_{0|k} - S_c^{-1} S_{cd} \underline{d}_{\rightarrow k} \quad (21)$$

Close inspection of (21) suggests that, to retain the closed-loop robust properties, the perturbation sequence $\underline{c}_{\rightarrow k}$ must be independent of the state $x_{0|k}$ (i.e. $S_{xc}^T = 0$ in the cost).

Theorem 1: The input perturbation sequence $\underline{c}_{\rightarrow k}$ in normal operation from the MPC additional layer has no impact on the original closed-loop dynamics if $S_{xc} = 0$. This can be

true only if the cost function in Algorithm 1 embeds some knowledge of the nominal output-feedback control law (10) such that the weights Q , R , N and S_x satisfy the following conditions:

$$\Phi^T S_x \Phi - S_x + Q + K^T R K = 0, \quad (22a)$$

$$B^T S_x \Phi + R K + N^T = 0. \quad (22b)$$

Proof: This is straightforward to demonstrate by investigating the cost function (17) and the Lyapunov equation $\Psi^T S \Psi = S - W$. ■

Corollary 1: This theorem is significant because it demonstrates that the extra MPC layer will not impact on the underlying robust closed-loop properties unless constraints are predicted to be active. Consequently, in normal operation, the properties of the underlying robust law are retained.

Nevertheless, a key point in the observation above is consistency between the performance index in Algorithm 1 and the underlying robust control law of (11b). Since the underlying controllers (10) employed in this work were designed using frequency-shaped technique, the weights that satisfy the conditions (22) can be determined by solving a linear matrix inequality (LMI) problem [15].

IV. NUMERICAL RESULTS AND DISCUSSIONS

This section demonstrates the efficacy and performance benefits of the use of the combined MPC/robust control structure by performing closed-loop simulations on a high-fidelity wind turbine model.

A. Simulation environment and settings

The turbine model employed in this study is the NREL 5MW turbine [16] based on the FAST code [17]. This model is of much greater complexity than the model (7) employed for control design and includes flap-wise and edge-wise blade modes, in addition to tower and drive train dynamics. The wind field generated by the TurbSim code [18] numerically simulates the time series of a three-dimensional wind vectors at points in a two-dimensional vertical rectangular grid such that the series of grids march towards the rotor specified by the mean wind speed and under the assumption of Taylor's frozen turbulence hypothesis. The upcoming stream-wise wind speed measurements on a 17-by-17 grid across the rotor plane were obtained from the TurbSim code. Nevertheless, the feed-forward inputs based on such turbulent wind measurements were aggressive and ineffective, thus, to remove the spatial turbulences that are less sensitive to turbine loads, the measurements of the turbulent wind field $v_m(y_r, z_r)$ can be reconstructed into a simplified wind field $v(y_r, z_r)$:

$$v(y_r, z_r) = \bar{v} + \delta_h y_r + \delta_v z_r \quad (23)$$

where y_r and z_r are the horizontal and vertical co-ordinates across the rotor plane. The averaged wind speed, horizontal and vertical shear components are denoted as \bar{v} , δ_h and δ_v , respectively, and these values were obtained on-line by performing least squares over the wind speed measurements $v_m(y_r, z_r)$ [19]. Subsequently, these simplified wind speed measurement would be employed in (6) to estimate the disturbance trajectories.

B. Tuning of the MPC layer

The predictive controller should anticipate the upcoming wind far enough ahead to allow beneficial feed-forward compensation; it was found that $n_a = 15$ samples was a reasonable choice in this simulation setting. The operating frequency of the MPC controller was 5 Hz which gives a good compromise between performance and computational burden; hence the preview horizon is 3 seconds ahead. It is clear that a similar idea also holds true for the control horizon n_c . The control horizon must be at least as large as the preview horizon, for the reason that the MPC controller can then plan effective control sequences to compensate for the wind disturbance.

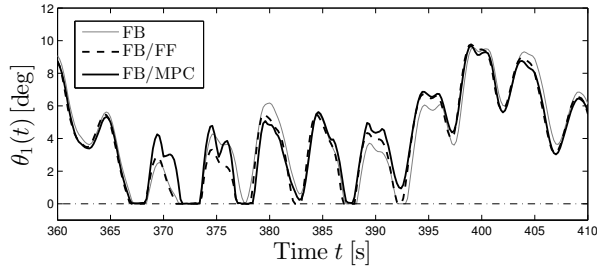
C. Simulation results

The closed-loop simulation was performed under a turbulent wind field characterised by the mean speed of 13 ms^{-1} and turbulence intensity of 14%. Three controllers were investigated: (i) the baseline robust feedback controller based on the control law (10) denoted as (FB); (ii) (FB/FF) represents the unconstrained additional layer on top of the baseline feedback compensator where the unconstrained input perturbation (21) is simply added to the feedback control law and (iii) the constraint-aware additional layer augmented with the embedded baseline feedback controller, where the input perturbation is computed on-line by solving Algorithm 1, denoted as (FB/MPC).

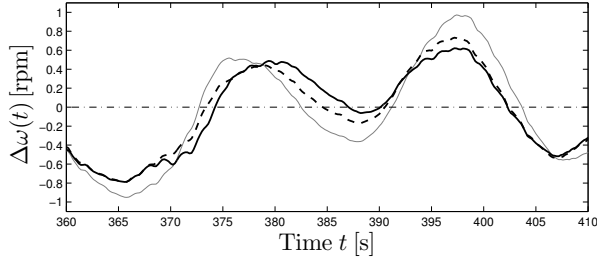
Figure 3 shows the sample time history excerpted from a 20-minute simulation result. Figure 3(a) illustrates the time history for the pitch angle of blade 1 where the controllers reached the pitch angle constraints and behaved differently. Consequently, in Figure 3(b), the rotor speed deviation for FB/MPC was slightly better than FB/FF. More importantly, Figure 3(c) shows significant reductions in flap-wise blade bending moment achieved by FB/MPC compared to FB/FF. The results from the full 20 minute simulation are summarised in Table I. As shown in Table I, it is not surprising that FB/FF and FB/MPC achieved lower standard deviations on rotor speed and blade load rejections compared to FB since they used of approaching wind measurements. Furthermore, the results showed that the constraint-aware controller FB/MPC also outperformed FB/FF slightly. The difference is not significant because violations of pitch actuator constraints were infrequent. It is surmised that better improvement could be achieved by FB/MPC if soft-constraints on rotor speed and blade loads were also included.

V. CONCLUSION

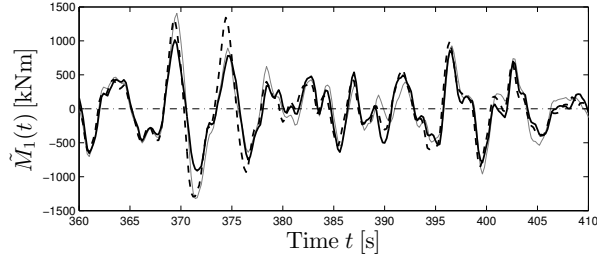
This work has shown the MPC layer design on top of a given output-feedback blade-pitch controller where the layer handles the upstream wind measurements and constraints. The conditions for separating the original closed-loop dynamics from the additional control design were also proposed in this paper. Such MPC layer design retains the robustness properties of the given feedback controller unless constraint violations are expected. Closed-loop simulations on a high-fidelity turbine were performed, showing the benefits gained



(a) Time history of the pitch angle of blade 1. Dash-dot lines represent the pitch angle constraint at 0 degree.



(b) Time history of the rotor speed deviation. Dash-dot line represents the targeted rotor speed.



(c) Time history of the flap-wise blade root bending moment of blade 1. Dash-dot line represents the targeted blade loads.

Fig. 3. Simulation results upon the NREL 5MW turbine, showing the performance of the various controllers studied in this paper.

TABLE I
CONTROLLER PERFORMANCE COMPARISONS

Description	FB (Baseline)	FB/FF	FB/MPC
std(ω) (rpm)	0.32 (100%)	0.27 (84%)	0.27 (84%)
std(M_1) (kNm)	629 (100%)	589 (94%)	581 (92%)
std($\dot{\theta}_1$) (deg s ⁻¹)	1.60 (100%)	1.56(98%)	1.56 (98%)

Note that std denotes the standard deviation. The percentage in bracket represents the relative difference to the baseline controller.

by the proposed MPC-based preview controller. Future work will include constraints on rotor speed and blade loads.

APPENDIX I

The model parameters for (7) are shown in Table II and the closed-loop robust controllers are described as follows:

$$K_{\theta\omega}(s) = \frac{10.74s + 3.845}{3.142s} \quad (24a)$$

$$K_{\theta M}(s) = 10^4 \times \frac{2.3s^4 + 6.1s^3 + 25.4s^2 + 18.1s + 39}{(s^4 + 0.20s^3 + 8.06s^2 + 0.46s + 10.38)} \quad (24b)$$

TABLE II
MODEL PARAMETER OF $G(s)$ (7)

Parameters	Values	Units	Parameters	Values	Units
$\frac{\partial\omega}{\partial\theta}$	-0.84 rpm deg ⁻¹		$\frac{\partial M_{flap}}{\partial\theta}$	-9.02×10^5 Nm deg ⁻¹	
τ_r	4	s	f_b	0.70	Hz
D_b	0.47	-	τ	0.11	s
f_h	0.80	Hz	f_l	0.014	Hz

REFERENCES

- [1] K. Selvam, S. Kanev, J. W. van Wingerden, T. van Engelen, and M. Verhaegen, "Feedback-feedforward individual pitch control for wind turbine load reduction," *International Journal of Robust and Nonlinear Control*, vol. 19, no. 1, pp. 72–91, 2009.
- [2] W. Leithead, V. Neilson, and S. Dominguez, "Alleviation of Unbalanced Rotor Loads by Single Blade Controllers," in *European Wind Energy Conference & Exhibition*, 2009.
- [3] D. Schlipf, T. Fischer, and C. Carcangiu, "Load analysis of look-ahead collective pitch control using LIDAR," in *Proc. of 10th German Wind Energy Conference*, 2010.
- [4] D. Schlipf, P. Fleming, F. Haizmann, A. Scholbrock, M. Hofsaß, A. Wright, and P. W. Cheng, "Field Testing of Feedforward Collective Pitch Control on the CART2 Using a Nacelle-Based Lidar Scanner," in *The Science of Making Torque from Wind*, 2012.
- [5] J. Laks, L. Pao, and A. Wright, "Combined Feed-forward/Feedback Control of Wind Turbines to Reduce Blade Flap Bending Moments," in *AIAA/ASME Wind Energy Symp.*, Orlando, FL, 2009.
- [6] J. Laks, L. Pao, E. Simley, A. Wright, N. Kelley, and B. Jonkman, "Model Predictive Control Using Preview Measurements From LIDAR," in *49th AIAA*. Reston, Virginia: American Institute of Aeronautics and Astronautics, 2011.
- [7] M. D. Spencer, K. A. Stol, C. P. Unsworth, J. E. Cater, and S. E. Norris, "Model predictive control of a wind turbine using short-term wind field predictions," *Wind Energy*, vol. 16, no. 3, pp. 417–434, 2013.
- [8] Wai Hou Lio, J. Rossiter, and B. L. Jones, "A review on applications of model predictive control to wind turbines," in *2014 UKACC International Conference on Control (CONTROL)*. Loughborough, U.K.: IEEE, 2014, pp. 673–678.
- [9] E. A. Bossanyi, "Individual Blade Pitch Control for Load Reduction," *Wind Energy*, vol. 6, no. 2, pp. 119–128, 2003.
- [10] Q. Lu, R. Bowyer, and B. Jones, "Analysis and design of Coleman transform-based individual pitch controllers for wind-turbine load reduction," *Wind Energy*, vol. 18, no. 8, pp. 1451–1468, 2015.
- [11] W. H. Lio, B. L. Jones, Q. Lu, and J. Rossiter, "Fundamental performance similarities between individual pitch control strategies for wind turbines," *International Journal of Control*, 2015.
- [12] P. Towers and B. L. Jones, "Real-time wind field reconstruction from LiDAR measurements using a dynamic wind model and state estimation," *Wind Energy*, vol. 19, no. 1, pp. 133–150, 2016.
- [13] J. A. Rossiter, *Model-Based Predictive Control: A Practical Approach*. CRC Press, 2003.
- [14] E. Gilbert and K. Tan, "Linear systems with state and control constraints: the theory and application of maximal output admissible sets," *IEEE Transactions on Automatic Control*, vol. 36, no. 9, pp. 1008–1020, 1991.
- [15] S. Boyd, L. El Ghaoui, E. Feron, and V. Balakrishnan, *Linear Matrix Inequalities in System and Control Theory*. Society for Industrial and Applied Mathematics, 1994.
- [16] J. Jonkman, S. Butterfield, W. Musial, and G. Scott, "Definition of a 5-MW Reference Wind Turbine for Offshore System Development," National Renewable Energy Laboratory (NREL), Golden, CO, Tech. Rep., 2009.
- [17] J. Jonkman and M. Buhl Jr, "FAST User's Guide," National Renewable Energy Laboratory (NREL), Tech. Rep., 2005.
- [18] B. Jonkman, "TurbSim User's Guide," National Renewable Energy Laboratory (NREL), Tech. Rep., 2009.
- [19] D. Schlipf, S. Schuler, P. Grau, and K. Martin, "Look-Ahead Cyclic Pitch Control Using LIDAR," in *The Science of Making Torque from Wind*, 2010.